

Novel Spark Plasma Extrusion of Titanium Above and Below the β -Transus: Effect on Microstructure and Properties



R. HALLETT, J.R. COX, and K. MORSI

Spark plasma extrusion is a new process that has recently shown superiority over spark plasma sintering for powder consolidation. This paper represents the first investigation of novel spark plasma extrusion (SPE) of titanium (Ti) powder. Extrusion temperature (above and below the β -transus) and initial Ti powder type were found to have a pronounced effect on the developed microstructures and properties. SPE conducted above the β -transus resulted in the formation of Widmanstätten microstructures in addition to martensitic α' upon cooling, which ultimately lead to superior product hardness. SPE processing, microstructure, and properties were found to be affected by the initial Ti powder used, where dendritic Ti powder resulted generally in lower extrusion pressures and products of lower hardness, compared to irregular/angular Ti powder. The results also confirm the superiority of SPE over SPS for Ti (irrespective of initial Ti powder type or extrusion temperature) as related to mechanical behavior.

<https://doi.org/10.1007/s11663-020-01845-5>

© The Minerals, Metals & Materials Society and ASM International 2020

I. INTRODUCTION

THE solid-state sintering of powders is one of the oldest consolidation processes for powder-based materials.^[1] However, recently, spark plasma sintering (SPS) has been under intense investigation as a process that promotes faster sintering rates, lower sintering temperatures, while using higher heating rates than conventional sintering in a furnace.^[2,3] These remarkable advantages are a result of the simultaneous application of electric current and pressure to powders. Despite its advantages, SPS has a number of limitations. One is the inability to impose process-induced recrystallization, which could normally allow microstructural refinement. Second is its inability to intrinsically and efficiently align reinforcements when sintering composite materials. Third is its fundamental inability to produce products of complex and extended geometries. From the scientific perspective, such limitations can also lead to the masking of intriguing scientific phenomena that can yield extraordinary insights, for example recrystallization under the influence of electric current, among others as explained below.

If instead of simply pressing powders under the influence of current and uniaxial pressure as in SPS, powders were subjected to shear deformation under electric current, a number of new benefits can be realized which can set the stage for novel scientific investigations. As such, novel spark plasma ‘extrusion’ (SPE) has been recently reported by one of the authors,^[4] which allows the ultra-rapid (orders of magnitude faster than SPS) consolidation of powders while under the influence of electric current. The process boasts several advantages over SPS, which include faster consolidation, electrically activated dynamic recrystallization leading to grain refinement, enhanced phase transformation kinetics, reinforcement alignment, and the production of materials with more complex and extended geometries.^[4] Apart from a recent publication on the current-assisted extrusion of Fe_{49.7}Cr_{17.7}Mn_{1.9}Mo_{7.4}W_{1.6}B_{15.2}C_{3.8}Si_{2.4} containing Y₂O₃ nanoparticles,^[5] so far, aluminum and aluminum-carbon nanotube materials have been the main material systems processed by SPE.^[6–8] Although these aluminum and aluminum carbon nanotube composites were successfully processed using SPE, however, they did not undergo any phase transformations at the extrusion conditions investigated. As such, the present paper investigates for the first time the effect of extrusion temperature above and below the β transus for Ti (reported to be ~ 882 °C to 950 °C depending on impurity content^[9]) on the product microstructure and properties.

R. HALLETT and K. MORSI are with the Department of Mechanical Engineering, San Diego State University, 5500 Campanile Dr., San Diego, CA 92182. Contact e-mail: kmorsi@sdsu.edu J.R. COX is with the Universal Achemetal Titanium, 109 South Parkmont, Butte, MT 59701.

Manuscript submitted December 31, 2019.

Article published online May 5, 2020.

II. EXPERIMENTAL PROCEDURES

Two titanium powders were investigated, commercially pure (CP-Ti) and a new low-cost (dendritic) titanium powder (UAT) produced by an environmentally friendly extraction process that does not liberate any greenhouse gasses.^[10] Commercially pure titanium powders CP-Ti [-325 mesh, Ti-104, Atlantic Equipment Engineers, and UAT Ti (UAT-Ti)] were used in the experiments. Figure 1 shows scanning electron micrographs of the powders. As can be seen the UAT powder is dendritic, while the CP-Ti displays an irregular/angular shape.

Both powders were compacted at room temperature to produce powder compacts (~ 19.2 mm diameter and ~ 29 long) with relative densities of ~ 0.64 compared with theoretical. The compacts were drilled centrally on the bottom face to allow the insertion of a k-type thermocouple. The compacts were placed in the spark plasma extrusion rig (Figure 2) with an electrically insulating inner liner. Two PowerTEN power supplies capable of applying current intensities up to 2000 A at 0 to 5 V were used for heating the powder compact to the extrusion temperature through Joule heating. Graphite powder was used as a high-temperature lubricant. Extrusion was conducted under an argon atmosphere at two different temperatures signifying extrusion temperatures in the α -Ti phase field (~ 806 °C ± 2 °C) and the β -Ti phase field (~ 1234 °C ± 10 °C). An extrusion speed of 16.48 mm/s was used in all cases. The high speed of extrusion was used to minimize heat losses from the compact to the container, which was originally maintained at room temperature (to be discussed later). Electric current was switched off as soon as the extrusion was complete. For all conditions, an extrusion ratio of 10:1 was used equivalent to a strain of 2.3. Extrudates were sectioned centrally along the extrusion direction, then ground, polished, and etched in Kroll's reagent for 20 seconds for microstructural characterization. Phase and microstructural analysis were conducted using X-ray Diffraction and field-emission scanning electron microscopy. For oxygen and nitrogen analysis, inert gas fusion was used per ASTM 1409-13. For all

other elements, direct current plasma emission spectroscopy was used per ASTM standard 2371-13. The localized mechanical response of the extruded materials was investigated using a microhardness tester using an indentation load of 1 kg.

III. RESULTS AND DISCUSSION

Since electric activation is an integral and unique part of SPE, some internal mechanisms are hence different than those found in regular hot extrusion, namely the relation between the electric resistance of the powder compact during consolidation and the corresponding heat generation term (through Joule heating as explained later). The micro- and macro-structural evolution during SPE can be viewed in light of the schematic shown in Figure 3. As shown in the figure, extrusion of the compacts occurs from top to bottom. The region referred to, as the discard is simply the material left behind in the container (un-extruded). Such leftover material can shed important light on the microstructural evolution inside the container prior to extrusion (*i.e.*, a spatial snapshot of the material immediately prior to extrusion). Initially as the compact

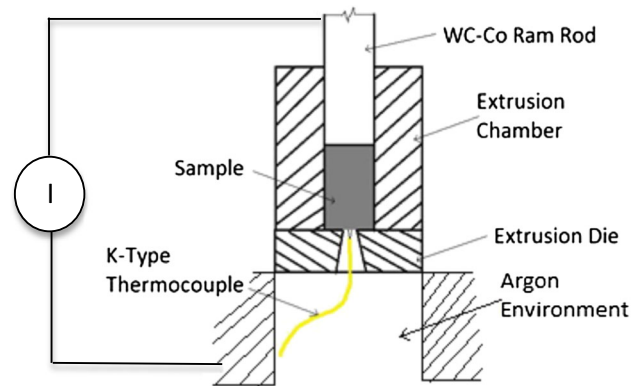


Fig. 2—Schematic of SPE setup.

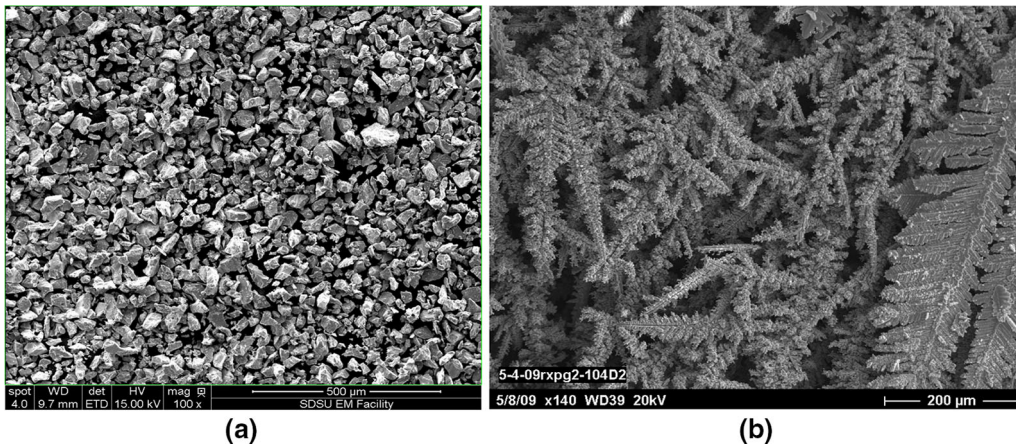


Fig. 1—(a) Scanning electron micrographs of (a) CP-Ti and (b) UAT-Ti powder.

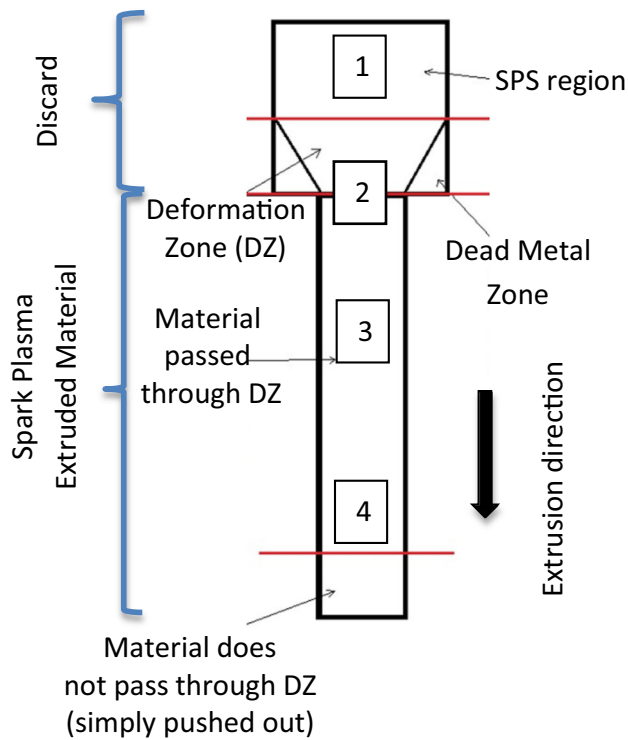


Fig. 3—Schematic of extrusion cross-section, showing discard region, extruded region, and locations (1 to 4) where microstructures and properties were investigated (note, material below the red line was not used in the analyses).

is pressed inside the extrusion container, the material is first consolidated under pressure with some upsetting which allows the compact to conform to the inner dimensions of the extrusion container. This is immediately followed by the extrusion of the material outside of the container through the smaller opening in the die. It is well known in hot extrusion that a number of features develop inside the container during extrusion. One is a deformation zone (DZ), which is a truncated cylindrical region (just above the die exit) where material is heavily sheared in order to reduce the cross-section. Surrounding the DZ in contact with the extrusion die and the inner liner of the container is the dead metal zone (DMZ) where material is stagnant. Above the deformation zone (in Figure 3) is material that is simply pushed down the extrusion chamber and subjected to compression under the influence of electric current. In fact what emerges is a very interesting scenario where one extrusion can produce regions within the material that is subjected to spark plasma sintering conditions (location 1) while the extruded part (locations 3 and 4) is subjected to spark plasma extrusion conditions, both, initially processed at the same temperature and pressure. Specifically, locations 1 to 4 (along the central line of the extrusion) represent the following conditions: 1. Spark Plasma Sintered Region, 2. Region at point of exit of die, 3. Spark plasma extruded region, and 4. spark plasma extruded region, but extruded prior to region 3. Note as shown in Figure 3, the very first

material to be extruded (tip of the extrudate) is simply pushed out of the die exit and does not pass through the deformation zone.

It is also important to point out that during SPE there are sources for heat generation and heat losses, with one particularly unique to SPE. Specifically, sources of compact heating include Joule heating (which depends on the electrical resistance of the powder compact, which will vary with the extrusion ram displacement) and the work of extrusion. The effect of Joule heating however is expected to diminish as the compact is densified further inside the container during the extrusion stroke. This is because the density of the compact will increase resulting in a decline in its electrical resistance.^[11] Moreover, due to the very good contact of the hot extruding compact and the colder inner container wall (initially maintained at room temperature), rapid heat losses are expected during extrusion due to heat conduction away from the hot compact to the container and die. The overall effect of these competing sources for our current setup is a decline in the compact temperature during extrusion.^[4] Hence in order to reduce excessive heat loss, the extrusion is carried out at a relatively high speed.

Figure 4 shows the extrusion pressure vs displacement curves during spark plasma extrusion of the CP-Ti and UAT-Ti powder compacts at two different extrusion temperatures.

The figure shows that an increase in the extrusion temperature results in a decline in extrusion pressure, due to the expected decline in flow stresses for both types of powder compacts. Additionally, the UAT-Ti powder compacts are found to require less extrusion pressure than the CP-Ti. Since an increase in oxygen and other impurity levels can significantly increase the strength of titanium,^[12] the UAT-Ti with its lower oxygen content compared to that of the CP-Ti used (explained later) results in a lower flow stress for UAT-Ti compared with CP-Ti, and hence the lower extrusion pressures observed. Additionally, the dendritic structure of the powders may have also facilitated powder flow (however further investigations are needed to confirm this).

The almost continuously increasing extrusion pressure with ram displacement is also a direct result of the decline in temperature during extrusion, as mentioned earlier.

For both UAT-Ti and CP-Ti, extrusions were conducted at initial extrusion temperatures within the α -Ti phase field (~ 806 °C), fir-tree type cracking is evident, which is caused by limited ductility at that temperature (Figures 5(a) and (b)). Such cracking is, however, absent at extrusion temperatures of 1234 °C as seen in Figures 5(c) and (d).

The microstructures of extrusions conducted above the β -transus contained a Widmanstatten structure (retained β -Ti), which was not observed when extrusion was conducted below the β -transus. Moreover in Figure 6 (an example for CP-Ti extruded above β -transus) appears to coarsen from locations 2 to 4. Noting that during spark plasma extrusion in the present configuration (*i.e.*, with a hot compact inside a container initially

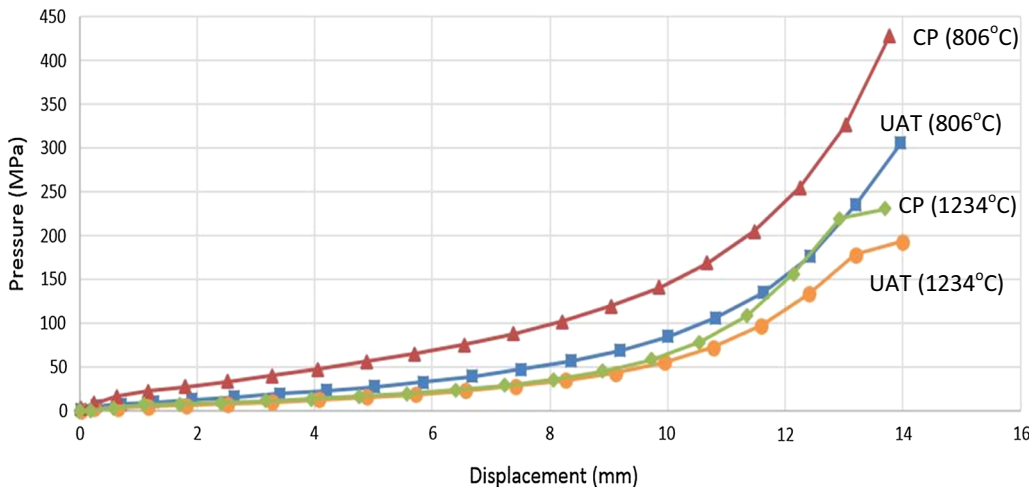


Fig. 4—Extrusion pressure vs ram displacement for CP-Ti and UAT-Ti at extrusion temperatures of 806 °C and 1234 °C.



Fig. 5—Extrudates extruded at temperatures in the α -Ti phase field (806 °C) (a) CP-Ti, (b) UAT-Ti, and in the β -Ti phase field (1234 °C) (c) CP-Ti and (d) UAT-Ti.

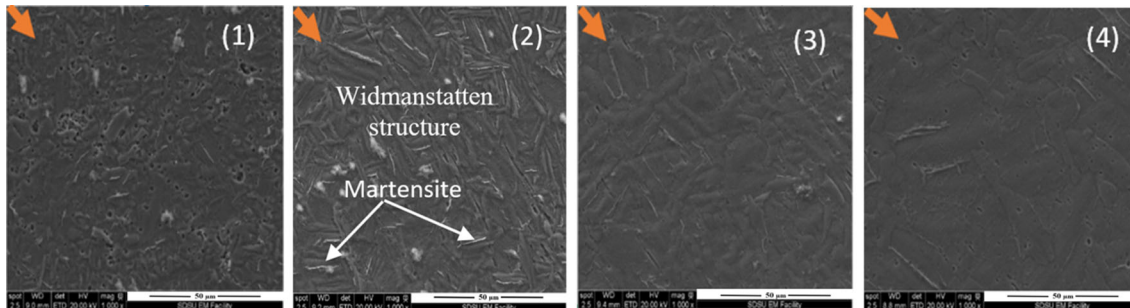


Fig. 6—Extrudate and microstructures at locations 1 to 4 along the extrusion direction for CP-Ti extruded at 1234 °C, arrows in the micrographs represent the extrusion direction relative to the microstructure (scale bars are 50 μ m).

at room temperature), the actual temperature at which the material is being extruded declines with ram displacement, due to heat loss from the compact to the cooler container.^[4] Consequently, it is expected that the first extruded material exiting the die would be at a higher temperature than subsequent parts of the extruding compact. If we examine the extrudate, materials in

locations 2 to 4 would have been initially extruded at increasingly higher temperatures going from 2 to 4. This explains the microstructural coarsening observed from 2 to 4 in Figure 6. Such variation in grain size along the extrudate length has been previously reported in hot extrusion,^[13] when the extrusion chamber is maintained at temperatures lower than the compact temperature

(which is the same in our case). What is also interesting is that microstructure from location 1 (*i.e.*, inside the extrusion chamber, and spark plasma sintered, Figure 3) did not clearly show the Widmanstatten structure.^[14] This is understandable since the larger compact with smaller surface area-to-volume ratio as compared to the thinner extruded material should cool at a lower rate. The formation of these Widmanstatten structures in the extruded material are further confirmed through XRD, where in Figure 7(a), α - and β -Ti peaks were present with some minor peak of martensite α' . This means that some of the β -Ti were retained at room temperature, due to the rapid cooling experienced following the material exiting the extrusion die. While both CP-Ti and UAT-Ti spark plasma extruded below the β -transus resulted in α -Ti at room temperature as expected (Figures 7(b) and (d)), the UAT-Ti spark plasma extruded at ~ 1234 °C (*i.e.*, within the β -Ti phase field) did not result in significant β -Ti being retained at room temperature contrary to the CP-Ti. This is reflected in only α -Ti peaks appearing in the XRD scans (Figure 7(c)), however, since XRD typically has a resolution of 3 vol pct, we cannot unequivocally discount the presence of β -Ti in small amounts.

In fact, Figure 8 indeed shows very minute amounts of retained β for UAT-Ti extruded at 1234 °C.

Yet, the marked difference between the resulting microstructures in both types of Ti extruded from the same β -Ti phase field needs further analysis as follows: From the extrusion pressure–ram displacement curves it is clear that the UAT-Ti is softer than the CP-Ti, *i.e.*, requiring lower extrusion pressures. This low flow stress and corresponding enhanced ductility should result in better conformability of the compact surface and contact with the inner liner of the extrusion chamber during compact upsetting and extrusion. Such enhanced contact should result in enhanced heat transfer from the hot compact to the colder extrusion chamber, leading to a rapid reduction in UAT-Ti temperature as compared with CP-Ti prior to the material exiting the extrusion die. In fact, analysis of the thermocouple readings after compact upsetting and at onset of extrusion shows that

the UAT-Ti temperature drops from ~ 1234 °C to 883 °C, as opposed to ~ 1234 °C to 1176 °C for the CP-Ti.^[14] Hence, the UAT-Ti compact is in fact closer to the β -transus upon extrusion, which explains the absence of significantly retained β -Ti.

Figure 9 shows microhardness values from location 4 for both temperatures. Understandably, the hardness of the UAT-Ti is lower than that of the CP-Ti due to its lower flow stress as explained earlier. The microhardness values are in line with recently reported values for CP-Ti processed through high-pressure torsion, and above the microhardness for an annealed CP-Ti (Hv 195).^[15] What is interesting is the increase in hardness observed due to the increase in extrusion temperature. This is a direct result of the formation of Widmanstatten structure and martensite. Despite the lower amount of such structures observed in the UAT-Ti extruded at 1234 °C, its finer

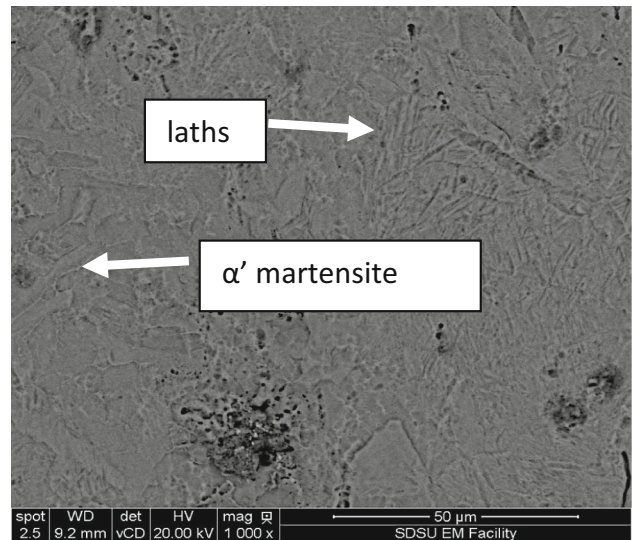


Fig. 8— α' martensite and lath structures in UAT-Ti extruded at 1234 °C.

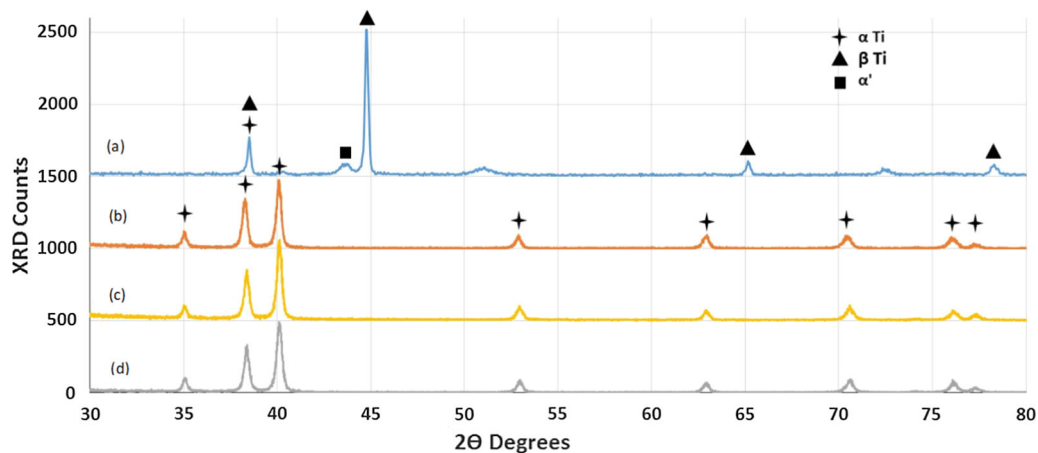


Fig. 7—XRD scans of spark plasma extruded CP-Ti and UAT-Ti above and below the β -transus, (a) CP-Ti 1234 °C, (b) CP-Ti 806 °C, (c) UAT-Ti 1234 °C, and (d) UAT-Ti 806 °C.

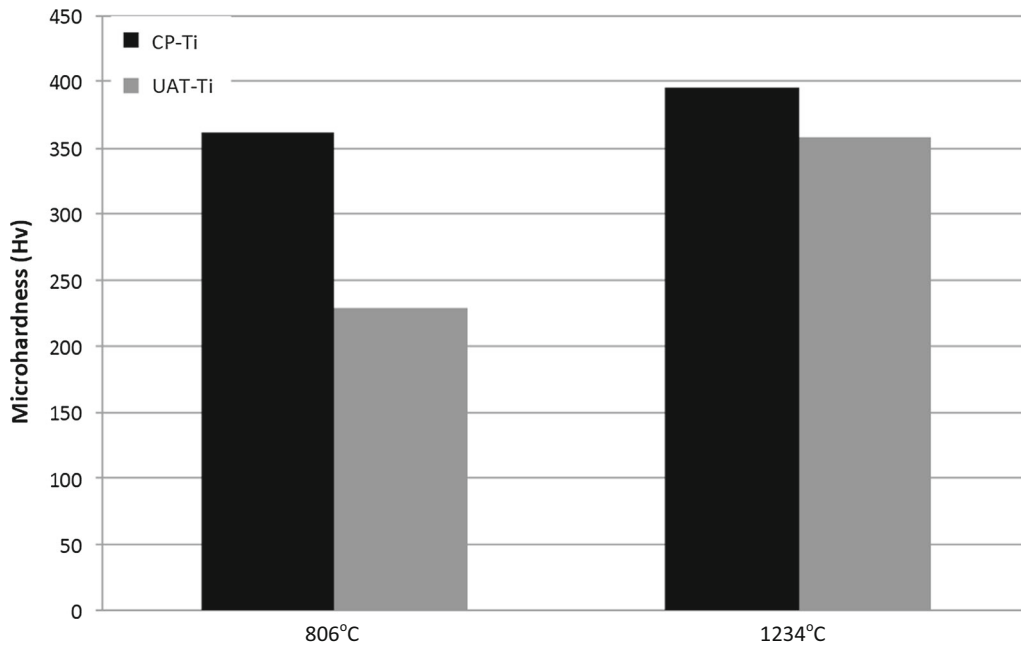


Fig. 9—Effect of Ti powder type and extrusion temperature on the microhardness of spark plasma-extruded materials (location 4).

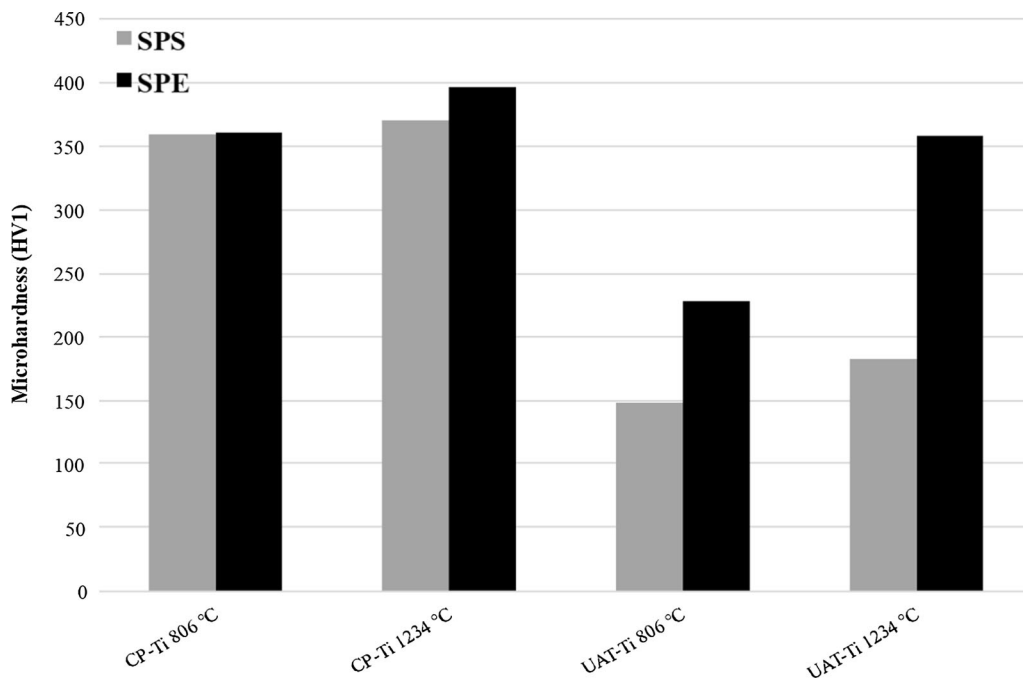


Fig. 10—Difference in microhardness between spark plasma-sintered Ti (location 1) and spark plasma-extruded Ti (location 4) for different extrusion temperatures and Ti powder.

structure (Figure 8) is expected to contribute to hardness more than that of a coarse structure for the CP-Ti (Figure 6). Hence, we observe a hardness of UAT-Ti that approaches that of CP-Ti at an extrusion temperature 1234 °C. Therefore, hardness is significantly affected by extrusion temperature, while powder type has a diminishing influence at the higher temperature.

Interestingly, irrespective of Ti powder type or extrusion temperature, microhardness values of titanium that have been spark plasma extruded (position 4) were higher than those taken from position 1 (*i.e.*, spark plasma sintered region, with reference to Figure 3) as seen in Figure 10. This is a result of the retention of β -Ti and martensite formation as mentioned earlier, while the

SPS region is expected to experience a lower cooling rate and hence less likely to form these phases. Additionally, an unusual observation was noted (which could have also contributed to the observed difference in hardness) such that elemental analyses of CP-Ti and UAT-Ti powder and post-SPE-extruded samples^[14] showed a general propensity for the CP-Ti to pick up significant oxygen (reaching around 0.8 pct from ~ 0.2 pct) following SPE as opposed to the UAT which remained almost the same at ~ 0.2 pct. Moreover, CP-Ti tended to also preferentially pick up aluminum (~ 0.3 pct), the source of which could be mica used as the thermal insulator within the extrusion container. Further work is however needed to fully elucidate such interesting findings, which should be the subject of a separate study.

IV. CONCLUSIONS

The following conclusions can be drawn.

1. Titanium powder has been successfully spark plasma extruded for the first time.
2. Irrespective of Ti powder type (CP or UAT), only extrusions conducted at 1234 °C were crack-free owing to increased ductility at that temperature.
3. UAT-Ti (with lower oxygen content) generally possessed lower hardness than the CP-Ti.
4. At higher extrusion temperature of 1234 °C, UAT-Ti possessed a hardness that approached that of CP-Ti extruded at the same temperature, presumably owing to the formation of observed finer-scale Widmanstätten structures.
5. Ti that was spark plasma extruded was harder than Ti that was spark plasma pressed irrespective of Ti powder type or extrusion temperature.

ACKNOWLEDGMENTS

The authors wish to thank Greg Morris for his assistance with the running of the spark plasma extrusion rig.

REFERENCES

1. R.M. German: *Powder Metallurgy & Particulate Materials Processing, Metal Powder Industry Federation*, 2005.
2. Z.A. Munir, U. Anselmi-Tamburini, and M. Ohyanagi: *J. Mater. Sci.*, 2006, vol. 41, pp. 763–77.
3. K. Morsi, M. Krommenhoek, and M. Shamma: *Metall. Mater. Trans. A*, 2016, vol. 47A, pp. 2574–78.
4. K. Morsi, A. El-Desouky, B. Johnson, A. Mar, and S. Lanka: *Scr. Mater.*, 2009, vol. 61, pp. 395–98.
5. E. Novitskaya, T.A. Esquivel-Castro, G.R. Dieguez-Trejo, A. Kritsuk, J.T. Cahill, S. Díaz-de-la-Torre, and O.A. Graeve: *Mater. Sci. Eng. A*, 2018, vol. 717, pp. 62–65.
6. K. Morsi, A.M.K. Esawi, P. Borah, S. Lanka, A. Sayed, and M. Taher: *Mater. Sci. Eng. A*, 2010, vol. 527, pp. 5686–90.
7. K. Morsi, A.M.K. Esawi, S. Lanka, A. Sayed, and M. Taher: *Composites Part A*, 2010, vol. 41, pp. 322–26.
8. L. Čelko, M. Menelaou, M. Casas-Luna, M. Horynová, T. Musálek, M. Remešová, S. Díaz de la Torre, K. Morsi, and J. Kaiser: *Metall. Mater. Trans. B*, 2019, vol. 50B, pp. 656–65.
9. G. Lütjering and J.C. Williams: *Titanium: Engineering Materials and Processes*, 2nd ed., Springer, Berlin, 2007.
10. J.Cox, C. DeAlwis, B. Kohler, M. Lewis, US Patent-US9816192B2: 2011.
11. R.M. German and S.J. Park: *Mathematical Relations in Particulate Materials Processing: Ceramics, Powder Metals, Cermets, Hard Materials, and Minerals*, Wiley, New York, 2008.
12. M.L. Wasz, F.R. Brotzen, R.B. McLellan, and A.J. Griffin: *Int. Mater. Rev.*, 1996, vol. 41, pp. 1–12.
13. K. Morsi, S.O. Moussa, and J.J. Wall: *J. Mater. Sci.*, 2005, vol. 40, pp. 1027–30.
14. R. Hallett: San Diego State University, MS Thesis, 2016.
15. M. Shirooyeh, J. Xu, and T.G. Langdon: *Mater. Sci. Eng. A*, 2014, vol. 614, pp. 223–31.

Publisher's Note Springer Nature remains neutral with regard to jurisdictional claims in published maps and institutional affiliations.